ARTICLE   OPEN

Check for updates

Ferroelectric order in hybrid organic-inorganic perovskite NH₄PbI₃ with non-polar molecules and small tolerance factor

Jia-Bin Li[1,2,3,7], Zhi-Kang Jiang[1,2,7], Rui Wang [4,5,6], Jin-Zhu Zhao [1,2,6✉] and Ruiqiang Wang[1,2✉]

The appropriate theoretical picture of describing the ferroelectric order in hybrid organic-inorganic perovskite remains attractive and under intense debate. We rationalize the interaction between organic molecule sublattice and inorganic frame from first-principles. Through systematic investigations on the NH₄PbI₃, we show that the non-polar octahedral rotation dominates the process of stabilizing of the lattice with small value of tolerance factor. The direct coupling between molecules is negligible. With the help of hydrogen bonding to the inorganic cage, molecule sublattice will eventually build long-range ferroelectric or anti-ferroelectric order under the constrain of the inorganic cage and further polarize the inorganic frame as the feedback. These results also clarify that to build ferroelectricity the polar molecule is helpful but not crucial. As the general rule for hybrid organic-inorganic perovskite, we identified the fundamental mechanism that can be considered as a critical pre-step forward to further controlling the related physics in functional materials.

INTRODUCTION

In recently years, hybrid organic-inorganic perovskites (HOIP) are a group of attractive materials that form a broad subclass of ABX₃ perovskites, in which the A- or X-site is occupied by organic molecules. Since the report of methylammonium lead iodide (CH₃NH₃PbI₃, or MAPbI₃) as one of the most promising materials for photovoltaic applications[1–13], whether HOIP, for instance the representative MAPbI₃, can be ferroelectric (FE) become a highly concentrated field. It is believed to be an important factor that can explain its nice efficiency[14–20]. However, although first-principles results indicated that its tetragonal phase favors a FE state[21–24], there still be plenty of debates and controversy results from both experiments and theory[25–33]. For instance, experimental signals of ferroelectricity are reported based on dielectric[34,35], quasielastic neutron scattering[36] and hysteresis loop measurements[37,38]. Besides, it was claimed that the observation of FE/ferroelastic domains in the polycrystalline films of MAPbI₃[39–41] The spontaneous polarization and its stability are, however, being questioned and with substantial discussions so far[42–46]. To better clarify this central issue requires not only further experimental measurements with higher accuracy but also the appropriate theoretical understanding of FE behavior in HOIP[47,48].

Comparing to conventional inorganic perovskites, the potential FE mechanism in HOIP is more complicated. On the one hand, the inorganic part is able to present prototypical "displacive" ferroelectrics. Their ferroelectricity is related to the ionic displacements while all the local dipoles form a long-range order corresponds to the condensation of the related polar phonon modes. On the other hand, molecules in HOIP usually have hydrogen saturated structures and connects with inorganic frame through hydrogen bonds. It will therefore introduce the "order-disorder" degree of freedom similar with the one in polyvinylidene difluoride (PVDF)[49]. In HOIP, it is necessary to consider not only these two degrees of freedom individually but also the interplaying between them as

one of the central mechanisms in HOIP. Therefore, substantial efforts have been made on exploring the extensive general rule of this issue in HOIP[50–55].

From the view of group theory while the local interaction is ignored, the sublattice of molecules in HOIP can be treated as an effective field which introduces additional symmetry comparing with the parent inorganic ABX₃ perovskites[56]. The ferroelectric order can be built via improper ferroelectric mechanism, with the help of which, the phenomenon (usually forbidden in their parent inorganic ABX₃ perovskites.) in several HOIP compounds are well explained such as [NH₄]Cd(HCOO)₃[57], [Gua]Cu(HCOO)₃[58–60], [Trz]Mn(H₂PO₂)₃[61], et al. Besides the macroscopic approach, on the one hand, it is believed that the polarity of molecule plays important role for the inversion symmetry breaking related behavior in HOIP, e.g. the polar MA⁺ molecules in the halide MAPbI₃[23,46,50,53]. On the other hand, it is also interesting to notice that the halide N(CH₃)₄SnI₃ is predicted to have FE ground state although the A site molecule is a non-polar one with the octupole moment[62]. It presents $R3m$ polar ground state and the behavior of which is similar to conventional proper ferroelectricity. All these tremendous progresses strongly imply that the corresponding global picture has not yet been accomplished.

We believe it is helpful to rationalize the FE or non-FE behavior in HOIP by using Goldschmidt tolerance factor $t = \frac{r_A + r_X}{\sqrt{2}(r_B + r_X)}$ [63] initially proposed in conventional inorganic perovskites where r_A, r_B and r_X are the radius of A, B and X atom, respectively. The tendency of being either ferroelectric or non-polar anti-ferro distortion can be estimated by the value of t. Generally, $t = 1$ leads to the ideal cubic perovskite structure. When $t > 1$, the A site atom is relatively large so that the system tends to develop a polar distortion; when $t < 1$, the A site atom become relatively small and the octahedra rotation will be favored. It is surprised to see that this empirical rule not only compatible with perovskites oxides[64] and halide perovskites[65,66] but also can be effectively extended to

¹Guangdong Provincial Key Laboratory of Quantum Engineering and Quantum Materials, School of Physics and Telecommunication Engineering, South China Normal University, Guangzhou 510006, PR China. ²Guangdong-Hong Kong Joint Laboratory of Quantum Matter, South China Normal University, Guangzhou 510006, PR China. ³Foshan (Southern China) Institute for New Materials, Foshan 528300, PR China. ⁴Institute for Structure and Function and Department of Physics, Chongqing University, Chongqing 400044, PR China. ⁵Center of Quantum Materials and Devices, Chongqing University, Chongqing 400044, PR China. ⁶Center for Computational Science and Engineering, Southern University of Science and Technology, Shenzhen 518055, PR China. ⁷These authors contributed equally: Jia-Bin Li, Zhi-Kang Jiang. ✉email: zhaojz@m.scnu.edu.cn; wangruiqiang@m.scnu.edu.cn

the HOIP. As it is mentioned above, the N(CH$_3$)$_4$SnI$_3$ show FE ground state which has larger value of tolerance factor ($t = 1.13$) due to the larger effective radius of A site N(CH$_3$)[62]. When the effective size of A site is relatively large, it behaves like an inorganic ion. In this case, the effect of hydrogen bonds, between molecules and the surrounding inorganic cage, is relatively weak comparing with the dominating size effect of molecules and ions. These results clearly suggest that polarity of molecules is not necessary for ferroelectric in HOIP and the compounds can behave as a proper ferroelectric perovskite material when $t > 1$.

In line with the discussions mentioned above, it is interesting to see what type of additional behavior will appear in HOIP with small values of tolerance factors. Since the A site molecule is relatively small that will have more "free" space for its motion in the local inorganic cage. When the molecule forms hydrogen bonds with its neighboring inorganic atom, it often displaces away from the geometric center of the local cage creating an effective local dipole. The local stable site is constrained by the shape of the inorganic BX$_3$ cage. This type of local dipole will further polarize the inorganic frame cage as well. Such origin of creating local dipole is not guaranteed but can be expected to be wildly exist in HOIP with $t < 1$. Therefore, which order the lattice shows depends not only on the configuration of molecule sublattice but also the way by which how it polarizes the inorganic frame. In other words, since the non-zero local dipole exist, the long-range FE or AFE order depends on the preference of the entire lattice. Distinguished with conventional inorganic perovskites, these mechanisms combine the order-disorder feature and ionic displacive phase transitions in a single HOIP materials and, furthermore, provide the opportunity to build a long-range FE or AFE order in a perovskite with small tolerance factor.

According to the analysis above, building FE order in a HOIP with small tolerance factor does not rely on the polarity of molecules. To confirm it, in this work, we will systematically study the behavior of ammonium lead iodide (NH$_4$PbI$_3$), choosing the non-polar NH$_4^+$ to replace the A site atom and molecule with respect to its counterpart CsPbI$_3$ and MAPbI$_3$, respectively. The effective radius of NH$_4^+$ (146)[67] is smaller than the ones of MA$^+$ (217)[67] and Cs$^+$ (178)[65] implying it is more "free" to displace in the inorganic cage having small tolerance factor ($t = 0.76$). By employing the first-principles calculations, we will show that NH$_4$PbI$_3$ presents orthorhombic ground state and tetragonal phase in the middle temperature range, similar with MAPbI$_3$ and CsPbI$_3$. Due to the interaction between NH$_4^+$ sublattice and the inorganic frame, cooperating with the intrinsic lattice dynamical properties of the inorganic frame, the tetragonal phase behaves as a FE one while the orthorhombic phase shows AFE order. Beyond the symmetry arguments, the essential role of the hydrogen bond will be highlighted in the global picture describing the behavior of HOIP.

RESULTS

Cubic phase

The NH$_4$PbI$_3$ has typical structure of perovskites. As it is shown in Fig. 1, the NH$_4^+$ occupies the A site and breaks the symmetry of the convention cubic perovskites. In our calculations, when the atomic positions of A, B and X site are pre-fixed at high-symmetric position, this cubic phase show 6.199 Å lattice constant. Significant structural instabilities are shown in its phonon dispersion curves. Besides the motion of ammonium itself, the ionic polar motion at Brillion Zone (BZ) center and the octahedral rotation modes at BZ boundary are unstable as well (the eigenvectors of the octahedral rotation modes are shown in Supplementary Fig. 1 of the Supplementary Information). When the position of A site NH$_4^+$ is relaxed, this molecule prefers to displace away from the geometric center of the PbI$_3$ cage and builds hydrogen bonds with its neighbor I atoms. This off-center motion will create a local dipole momentum. When all the Pb and I atoms are artificially
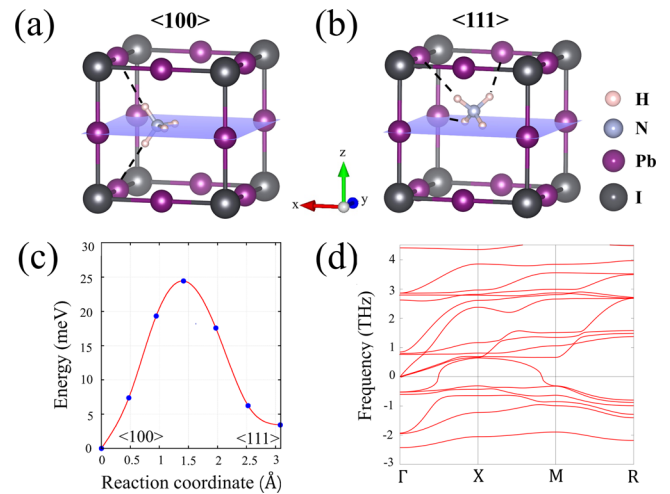

Fig. 1 The atomic structure and related dynamical behaviors of the cubic phase. The cubic phase of NH$_4$PbI$_3$ with inorganic Pb and I atoms fixed at high-symmetric position and displaced NH$_4^+$ molecule along concerned directions which are **a** <100> and **b** <110> directions, respectively. The hydrogen bonds are highlighted by the black dashed line. **c** The energy evolution in terms of the transition from <100> to <111> configuration obtain by CI-NEB calculations. **d** The phonon dispersion curves of cubic phase in which the NH$_4^+$ molecule is fixed at the high-symmetric site. The negative value of frequencies corresponds to the unstable phonon modes.

fixed at ideal high-symmetric positions, the molecule prefers to move along <100> and <111> direction forms two local stable configurations. These two motions reduce the total energy of 137 meV and 133 meV per p(1 × 1 × 1) formula unit, respectively while the formed hydrogen bonds are highlighted in Fig. 1. As we reported in Table 1, when all the atomic positions are fully relaxed, the inorganic PbI$_3$ cage will be further polarized by reducing additional ~60 meV/f.u. of the total energy, switching the polarization direction with value of (11.6, 6.7, 0.0) μC/cm^2.

The cubic phase has much higher energy than the distorted tetragonal and orthorhombic phase and therefore to be considered as the high-temperature phase. it is worth to mention that (1) according to the cubic symmetry, there are several equivalent sites that NH$_4^+$ favors to build hydrogen bonds with PbI$_3$ cage in a p(1 × 1 × 1) unit cell, which are six sites for <100> direction and eight sites for <111> directions, respectively. Our DFT results shows that the switching between them will have < 25 meV for energy barrier, obtained via CI-NEB method, that can be easily covered by thermal fluctuation at high temperatures. (2) The ferroelectric order in calculated p(1 × 1 × 1) unit cell represents the case that the long-range FE order in the whole lattice in which every unit cell have the same direction of local dipole. When we optimized the position of molecules in a p(2 × 1 × 1) supercell, the direction of two local dipoles favor to be perpendicular to each other and reduce the total energy of 21 meV/f.u. Further testing calculations (see Section II of the Supplementary Information) confirm that the direct coupling between two neighboring local dipoles is very weak and hardly to build long-range order against finite temperatures in cubic phase. Therefore, the order of molecule sublattice in cubic phase is not a stable ideal one under finite temperatures, but the one should be treated as a dynamical average of each energetical equivalent configurations. The NH$_4^+$ molecule will not stay in a certain site but continuously jump between each local stable site where the thermal average of total polarization is estimated to be zero. Thus, the whole lattice of cubic phase will be in a fully disordered state in which no stable long-range FE or AFE order can be expected. Here, we suggest considering this cubic phase as a theoretical model mainly for us to analyze the physics and hardly to be observed experimentally.

Table 1. The corresponding energy and polarization of selected phases and configurations.

	Energy gain (meV/f.u.)	Direction of local dipole	Fixed inorganic frame		Relaxed inorganic frame	
			Polarization (uC/cm^2)	Add. energy gain (meV/f.u.)	Polarization (uC/cm^2)	Add. energy gain (meV/f.u.)
Cubic	0	<100>	(10.4, 0.0, 0.0)	−137	(11.6, 6.7, 0.0)	−191
		<111>	(6.5, 6.5, 6.5)	−133	(11.6, 6.7, 0.0)	−192
Tetragonal	−410	T1 <111>	(3.2, 3.2, 3.2)	−80	(4.4, 4.4, 4.4)	−109
		T2 <111>	(1.6, 1.6, 1.4)	−74	(1.5, 3.2, 2.0)	−106
		T3 <111>	(0.0, 0.0, 0.0)	−68	(0.0, 0.0, 0.0)	−106
		T4 <111>	(0.0, 0.0, 0.0)	−65	(0.0, 0.0, 0.0)	−101
		T5 <111>	(0.0, 0.0, 0.0)	−80	(0.0, 0.0, 0.0)	−91
Orthorhombic	−367	<110>	(0.0, 0.0, 0.0)	−226	(0.0, 0.0, 0.0)	−236

The total energy of the related structure where only inorganic octahedral rotation is included are reported in the second column. In these structures, the NH_4^+ molecules are artificially fixed at the geometric center of the inorganic local cage and the position of H atoms are relaxed. The energy gain (in meV) is the value by taking the one of the cubic phases as the reference in which all the Pb, I and NH_4^+ molecules are at the high-symmetric sites. The "Add. Energy gain" in the sixth and eighth columns refer the energy difference by taking the structures in the second column as the reference introduced by the displacement of molecules and polarizations.

Tetragonal phase

The octahedral rotation will significantly reduce the total energy of NH_4PbI_3 and the structure of which will transits to a tetragonal phase. The out-of-phase rotation emergences in a p($\sqrt{2} \times \sqrt{2} \times 2$) supercell and show the $a^-a^-c^-$ configuration(in Glazer notation[68]) with the lattice constant of $a = b = 8.527$ Å and $c = 12.313$ Å. Due to its small value of the tolerance factor, the rotation angle of PbI_3 octahedral is as large as 10, 10 and 12 degree along x, y, z directions, respectively, which is comparable with the ones in $CsPbI_3$ and $MAPbI_3$. Such distortion not only reduce the total energy by 1.642 eV for each p($\sqrt{2} \times \sqrt{2} \times 2$) supercell, but also strongly changes the shape of the local PbI_3 cage and therefore re-evaluate the local stable site of NH_4^+ molecule. In the $a^-a^-c^-$ type distortion, the NH_4^+ connects with the cage via three hydrogen bonds and the length of which are 2.52, 2.52 and 2.55 Å, respectively (shown in Fig. 2b, c). Similar with the case of the cubic cage, the molecular displaces 0.66 Å away from the center of the cage forming a non-zero local dipole with 5.4 µC/cm^2 along <111> direction. Such off-center displacement will reduce the total energy by ~77 meV per each single molecule. There are two energetically equivalent local stable sites for NH_4^+ in a single PbI_3 cage, forming opposite local dipoles along its diagonal <111> and $<\overline{111}>$ direction of the local cage, respectively. For the convenience of the following discussions, these two sites are labeled as T+ and T− for <111> and $<\overline{111}>$ directions, respectively.

As it is discussed above, how NH_4^+ sublattices polarize the inorganic frame depends on the way of the arrangement order of these local dipoles. First, we check the preference order of NH_4^+ sublattice in the representative p($\sqrt{2} \times \sqrt{2} \times 2$) supercell without any additional distortion of PbI_3 in central symmetric $a^-a^-c^-$ configuration. As it is reported in Table 1 the energetical favorable order is a FE state, labeled as T1, in which all the NH_4^+ displaces along <111> direction. Such parallel arrangement of local dipoles will reduce total energy by ~320 meV in the supercell (around 80 meV per each dipole). There are four other in-equivalent configurations, shown in Fig. 2d, where local dipoles are in full or partial anti-parallel alignment. Comparing to the FE type, the rest ones show higher energy values. Further analysis shows that only the anti-parallel order alignment along <111> direction will gain the total energy while each anti-parallel-pairs along <111> will increase the energy by 25–30 meV (estimated in the p($\sqrt{2} \times \sqrt{2} \times 2$) supercell). It can explain the fact that the T5 configuration has almost the same energy with the FE one since anti-parallel-pairs in T5 are ordered along both <001> and <100> directions. Besides the T1, T2 and its equivalent configurations also present net polarizations.
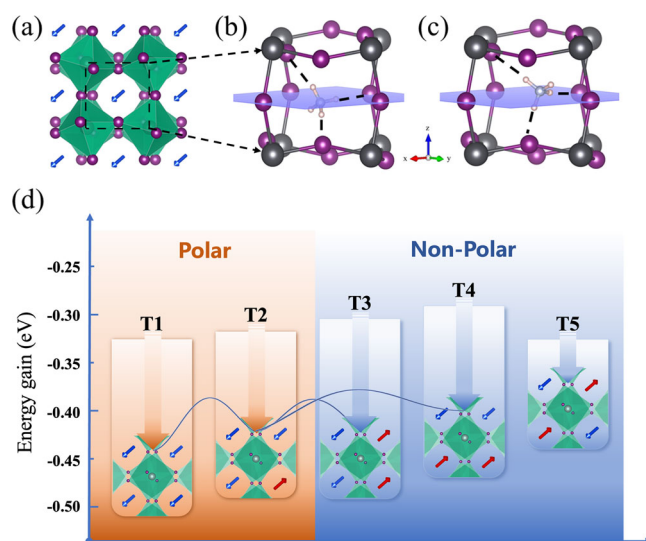

Fig. 2 The atomic structure and energy landscape for configurations of tetragonal phase. a The sideview of tetragonal phase of NH_4PbI_3 showing <111> polarization with $a^-a^-c^-$ type of octahedral rotation where the octahedrons are highlighted by green. The two energetical equivalent two local favorable sites for NH_4^+ molecule in single cage of tetragonal phase are shown in **b** with <111> polarization and **c** with $<\overline{111}>$ polarization, respectively. The hydrogen bonds are highlighted by the black dashed line. The highlighted plane with purple color is through the geometric center of the local cage. **d** The in-equivalent five configurations for the different alignment of the local dipoles where the direction of which is shown by blue and red arrows. The energy gain of each configuration in supercell are shown, by taking the one of un-displaced NH_4^+ molecule at the geometric center as the reference. Polar states and non-polar states are differed by the color of orange and blue, respectively. The top edge of each block corresponds to the energy value of the case that that NH_4^+ molecules are displaced while only $a^-a^-c^-$ type of octahedral rotations are included. When all the inorganic atoms are allowed to relax in each configuration, the corresponding energy reduction are highlighted by the arrows. The phase transition path and the corresponding energy barrier between each two investigated configurations are plotted by the blue curves between them.

Although the FE order configuration presents the lowest energy among these five, the energy fluctuation of them is limited below 80 meV (in supercell). When the inorganic ions, Pb and I, are allowed to relax their atomic position in these five configurations, the
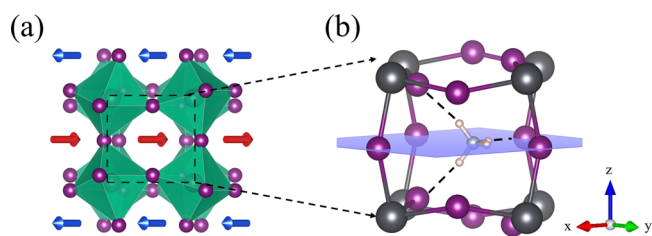
(a) (b)

Fig. 3 The atomic structure for orthorhombic phase. a The sideview of orthorhombic phase of NH_4PbI_3 showing <110> polarization with $a^-a^-c^+$ type of octahedral rotation where the octahedrons are highlighted by green. The alignment of the local dipoles the direction of which is shown by blue and red arrows. **b** The energetical local favorable sites for NH_4^+ molecule in single cage of orthorhombic phase with <110> polarization. The hydrogen bonds are highlighted by the black dashed line. The highlighted plane with purple color is through the geometric center of the local cage.

inorganic framework will be polarized and therefore the total energy will be further decreased more than 110 meV in the supercell. The gain of the total energy due to the ionic relaxation are reported in Table 1. Again, the FE T1 configuration is the most stable one with lowest energy. In consistent with the molecular sublattice, the inorganic cage prefers to be polarized along <111> direction. Besides, T2 configurations presents lower total energy than those with full anti-polar ordered configurations as well. As it is highlighted in Fig. 2d, to switch from the polar T1 phase to T2 phase, a ~70 meV energy barrier needs to be covered. As the next step, to switch the lattice from T2 phase to the non-polar T3 or T4 phase, ~50 meV is required. This energy cost corresponds to flipping the direction of one local dipole. Therefore, the tetragonal phase is estimated to present non-zero net polarization under finite temperatures.

Orthorhombic phase

Similar with the out-of-phase octahedral rotations in tetragonal phase, the in-phase rotation also reduces the total energy from the cubic phase by 1.466 eV for each $p(\sqrt{2} \times \sqrt{2} \times 2)$ supercell and drives the lattice to a $a^-a^-c^+$ phase. This value of energy gain, which is smaller than the one in tetragonal phase, is obtained by only considering the inorganic octahedral rotations while the molecules are artificially fixed at the high-symmetric sites. The rotation angle of PbI_3 octahedral is as large as 10, 10 and 12 degree along x, y, z directions, respectively, while the lattice constant is changed to $a = 8.396$ Å, $b = 8.401$ Å and $c = 12.216$ Å. Such lattice distortion constrains the local atomic environment in PbI_3 cage making the NH_4^+ displaces away from the symmetric center of the cage. As we present in Fig. 3, the local stable site of NH_4^+ is about 0.63 Å away from the cage center and provide 5.2 µC/cm^2 polarization along <110> direction of the local cage. Further studies show that there is only one favorable site in each cage for NH_4^+ forming three hydrogen bonds with the length of 2.56, 2.50 and 2.56 Å, respectively.

The alignment of the molecule sublattice in orthorhombic phase prefers a C-type anti-ferro order. As it is shown in Fig. 3a, when chose the c-axis as the out-of-plane direction, all the molecules form an in-plane FE order along <110> directions. All the local dipoles build anti-ferro order along the out-of-plane direction, align alternatively along <110> and <$\overline{1}\overline{1}0$> direction respectively. The formation of such anti-ferro order of molecule sublattice is fully determined by the local stable site of NH_4^+ molecules in each cage and originated from the constrain of the $a^-b^-c^+$ type octahedral rotation. Comparing to the ideal $a^-b^-c^+$ phase, the anti-ferro ordering of molecule sublattice will reduce the total energy of 226 meV/f.u. Similar with the case of tetragonal case, the local dipole built by the off-center displacement of NH_4^+ will further polarize the inorganic PbI_3 frame reduce 10 meV/f.u. in total energy. These additional displacements of Pb and I atom also form

an anti-ferro order in consistence with the molecule sublattice and eventually provide the global ground state of the lattice.

DISCUSSIONS

The results shown above indicate that the FE or AFE order in NH_4PbI_3 does not from neither the inorganic frame nor the organic molecule sublattice individually. On the one hand, similar with its counterparts $CsPbI_3$ and $MAPbI_3$, the inorganic frame of NH_4PbI_3 present *Pnma* ground state corresponding to the small tolerance factor. Tracing back to the phonon dispersion curve of the high-symmetric cubic phase, the octahedral rotations show strong lattice instabilities at the boundary of the Brillion zone. The condensation of these modes builds periodic non-polar long-range order in the lattice and significantly reduce the total energy. The conventional FE order driven by the phonon instabilities are suppressed by the octahedral rotations. On the other hand, due to the weak neighboring coupling between organic molecules, the arrangement of non-polar NH_4^+ sublattice is not able to build a stable long-range order individually but tends to be a fully disordered picture especially under finite temperatures.

Non-zero local dipole comes from the off-center displacement of NH_4^+ in each local cage. The energetically favored site of molecules relies on the shape of inorganic PbI_3 cage through the hydrogen bonds and often have several certain choices. The stability of such local dipole strongly depends on the constrain effects of the inorganic cage. For instance, due to the octahedral rotation the T+ and T− site for NH_4^+ in tetragonal is much more stable than the ones in cubic case. As the consequence, the inorganic local cage will be polarized along some certain directions. Thanks to the long-range ordered inorganic frame, by constraining the molecules the arrangement of the non-zero local dipole is able to build relative stable long-range FE or AFE order in lattice. The preference of inorganic frame eventually dominates the FE or AFE order for the whole lattice. For instance, as it is reported in Fig. 2d, although the T1 and T5 configuration for the molecule alignments presents similar energy gain, the $a^-a^-c^-$ type of octahedron rotation prefers FE type polarization rather than the AFE type. Therefore, the additional energy gain due to the displacement of inorganic atoms of T1 is much larger than the one of T5.

According to the analysis above, the FE phase in HOIP materials does not relies on the polarity of the molecules at the A site. In consistent with previous reports, polar molecule at A site in HOIP is not crucial but helpful that will support the existence of FE phase and further stabilize the polar order. This is a quite general mechanism for the HOIP materials since the hydrogen bond effect is wildly exist in these group of materials. For instance, it is nicely compatible with the case of the $MAPbI_3$, in line with several previous report[24,53]. Besides, our additional studies on the tetragonal structure of $CsPbI_3$ and dipole inter-molecular interactions of NH_4PbI_3 are reported in the Sections III and IV, respectively, of Supplementary Information further confirm that the hydrogen bond is the origin of the local dipole. According to the intrinsic nature of the hydrogen bond, the FE or AFE order in HOIP with small tolerance factor may not be stable at high temperatures since the hydrogen bond can be easily broken so that the sublattice will switch to a disordered state. We can also estimate that it will be easier to polarize the molecule sublattice or even the whole lattice of HOIP that is helpful for relating applications. Indeed, with the small tolerance factor, the stable perovskite structure of NH_4PbI_3 has not been experimentally observed up to now. The non-polar feature of its A site NH_4^+ molecule is a nice example and at least can be a representative theoretical model that avoid the intrinsic polarity of the molecules.

In conclusion, by showing the FE and the AFE phase of HOIP NH_4PbI_3 with non-polar A site molecule, we clarify the subtle and crucial role of the hydrogen bond between organic molecule and inorganic frame of the lattice. Our results confirmed that the

condensation of the long-range periodic phonon modes dominates the lattice distortion and strongly constrain the local cage of PbI_3. It therefore decides the local stable site of organic molecule through the optimizing of the hydrogen bond and build long-range order for the sublattice of A site molecules. The local dipole introduced by the off-center-displacement of the molecule will further polarize the lattice and produce the ground state of the lattice with the preference FE or AFE distortion of the inorganic frame. As we discussed, the proposed mechanism not only nicely works for the studied NH_4PbI_3, but also compatible with the case like the counterpart $MAPbI_3$. The general mechanism of the interplaying between organic sublattice and inorganic frame through hydrogen bonds as the media is built from viewpoint beyond the symmetry arguments and can be extended to broader field of organic-inorganic materials.

METHOD

In our investigations, we perform density functional theory (DFT)[69,70] calculations by employing the Vienna ab initio Simulation Package (VASP)[71,72], in which a plane wave basis set is used to expand the wave functions with a cut-off energy of 500 eV. The interactions between nuclei and the valence electrons are described by the projector augmented wave (PAW) method[73,74]. Interactions between valence electrons are counted by the generalized gradient approximation (GGA) with the PBEsol formalism[75–77]. The $6 \times 6 \times 6$ k-point mesh in Brillion Zone for formula unit cell and equivalent density for supercell is used. The crystal structures are fully relaxed until the residual force on each atom is below 10^{-3} eV/Å. The vibrational spectra are simulated through the phonopy code package[78,79] with inter-atomic forces calculated from VASP to evaluate its dynamical stability. The macroscopic polarization is calculated using the Berry phase method[80,81]. To study the reaction path between phases, the climbing image nudged elastic band (CI-NEB) method is used to investigate the minimum reaction pathways[82]. The so-called D3 correction method is applied as the approximation of van der Waals interactions[83].

DATA AVAILABILITY

All data used in this study are available from the corresponding author upon reasonable request.

REFERENCES

1. Quarti, C. et al. Structural and optical properties of methylammonium lead iodide across the tetragonal to cubic phase transition: implications for perovskite solar cells. *Energy Environ. Sci.* **9**, 155–163 (2016).
2. Ziffer, M. E., Mohammed, J. C. & Ginger, D. S. Electroabsorption spectroscopy measurements of the exciton binding energy, electron-hole reduced effective mass, and band gap in the perovskite $CH_3NH_3PbI_3$. *ACS Photonics* **3**, 1060–1068 (2016).
3. Ball, J. M. et al. Optical properties and limiting photocurrent of thin-film perovskite solar cells. *Energy Environ. Sci.* **8**, 602–609 (2015).
4. Stranks, S. D. et al. Electron-hole diffusion lengths exceeding 1 micrometer in an organometal trihalide perovskite absorber. *Science* **342**, 341–344 (2013).
5. Wehrenfennig, C., Eperon, G. E., Johnston, M. B., Snaith, H. J. & Herz, L. M. High charge carrier mobilities and lifetimes in organolead trihalide perovskites. *Adv. Mater.* **26**, 1584–1589 (2014).
6. Xing, G. C. et al. Long-range balanced electron- and hole-transport lengths in organic-inorganic $CH_3NH_3PbI_3$. *Science* **342**, 344–347 (2013).
7. McGehee, M. D. Continuing to soar. *Nat. Mater.* **13**, 845–846 (2014).
8. Yang, W. S. et al. Iodide management in formamidinium-lead-halide-based perovskite layers for efficient solar cells. *Science* **356**, 1376–1379 (2017).
9. Li, W. et al. Chemically diverse and multifunctional hybrid organic-inorganic perovskites. *Nat. Rev. Mater.* **2**, 1–18 (2017).
10. Zheng, X. et al. Managing grains and interfaces via ligand anchoring enables 22.3%-efficiency inverted perovskite solar cells. *Nat. Energy* **5**, 131–140 (2020).
11. Maiti, A. & Pal, A. J. Carrier recombination in $CH_3NH_3PbI_3$: why is it a slow process? *Rep. Prog. Phys.* **85**, 024501 (2022).
12. Even, J., Pedesseau, L., Jancu, J. M. & Katan, C. Importance of spin-orbit coupling in hybrid organic/inorganic perovskites for photovoltaic applications. *J. Phys. Chem. Lett.* **4**, 2999–3005 (2013).
13. Stroppa, A., Barone, P., Jain, P., Perez-Mato, J. M. & Picozzi, S. Hybrid improper ferroelectricity in a multiferroic and magnetoelectric metal-organic framework. *Adv. Mater.* **25**, 2284–2290 (2013).
14. Grinberg, I. et al. Perovskite oxides for visible-light-absorbing ferroelectric and photovoltaic materials. *Nature* **503**, 509–512 (2013).
15. Frost, J. M. et al. Atomistic origins of high-performance in hybrid halide perovskite solar cells. *Nano Lett.* **14**, 2584–2590 (2014).
16. Liu, S. et al. Ferroelectric domain wall induced band gap reduction and charge separation in organometal halide perovskites. *J. Phys. Chem. Lett.* **6**, 693–699 (2015).
17. Zheng, F., Tan, L. Z., Liu, S. & Rappe, A. M. Rashba spin-orbit coupling enhanced carrier lifetime in $CH_3NH_3PbI_3$. *Nano Lett.* **15**, 7794–7800 (2015).
18. Quarti, C., Mosconi, E. & De Angelis, F. Interplay of orientational order and electronic structure in methylammonium lead iodide: implications for solar cell operation. *Chem. Mat.* **26**, 6557–6569 (2014).
19. Wang, P. Q. et al. Photo-induced ferroelectric switching in perovskite $CH_3NH_3PbI_3$ films. *Nanoscale* **9**, 3806–3817 (2017).
20. Hu, S. B. et al. Dipole order in halide perovskites: polarization and rashba band splittings. *J. Phys. Chem. C.* **121**, 23045–23054 (2017).
21. Stroppa, A., Quarti, C., De Angelis, F. & Picozzi, S. Ferroelectric polarization of $CH_3NH_3PbI_3$ perovskite: a detailed study based on density functional theory and symmetry mode analysis. *J. Phys. Chem. Lett.* **6**, 2223–2231 (2015).
22. Brivio, F. et al. Lattice dynamics and vibrational spectra of the orthorhombic, tetragonal, and cubic phases of methylammonium lead iodide. *Phys. Rev. B* **92**, 144308 (2015).
23. Quarti, C., Mosconi, E., & De Angelis, F. Interplay of orientational order and electronic structure in methylammonium lead iodide: implications for solar cell operation. *Chem. Mater.* **26**, 6557–6569 (2014).
24. Tong, W. Y., Zhao, J. Z. & Ghosez, P. Missed ferroelectricity in methylammonium lead iodide. *npj Comput. Mater.* **8**, 165 (2022).
25. Fan, Z. et al. Ferroelectricity of $CH_3NH_3PbI_3$ perovskite. *J. Phys. Chem. Lett.* **6**, 1155–1161 (2015).
26. Ong, K. P., Goh, T. W., Xu, Q. & Huan, A. Mechanical origin of the structural phase transition in methylammonium lead iodide $CH_3NH_3PbI_3$. *J. Phys. Chem. Lett.* **6**, 681–685 (2015).
27. Gómez, A., Wang, Q., Goñi, A. R., Campoy-Quiles, M. & Abate, A. Ferroelectricity-free lead halide perovskites. *Energy Environ. Sci.* **12**, 2537–2547 (2019).
28. Guo, H. et al. Re-entrant relaxor ferroelectricity of methylammonium lead iodide. *Curr. Appl. Phys.* **16**, 1603–1606 (2016).
29. Sharada, G. et al. Is $CH_3NH_3PbI_3$ polar. *J. Phys. Chem. Lett.* **7**, 2412–2419 (2016).
30. Alvar, M. S., Kumar, M., Blom, P. W. M., Wetzelaer, G. J. A. H. & Asadi, K. Absence of ferroelectricity in methylammonium lead iodide perovskite. *AIP Adv.* **7**, 095110 (2017).
31. Filippetti, A., Delugas, P., Saba, M. I. & Mattoni, A. Entropy-suppressed ferroelectricity in hybrid lead-iodide perovskites. *J. Phys. Chem. Lett.* **6**, 4909–4915 (2015).
32. Seol, D. et al. Origin of hysteresis in $CH_3NH_3PbI_3$ perovskite thin films. *Adv. Funct. Mater.* **27**, 1701924 (2017).
33. Chen, H. W., Sakai, N., Ikegami, M. & Miyasaka, T. Emergence of hysteresis and transient ferroelectric response in organo-lead halide perovskite solar cells. *J. Phys. Chem. Lett.* **6**, 935–935 (2015).
34. Juarez-Perez, E. J. et al. Photoinduced giant dielectric constant in lead halide perovskite solar cells. *J. Phys. Chem. Lett.* **5**, 2390–2394 (2014).
35. Anusca, I., Balčiūnas, S. & Gemeiner, P. Dielectric response: answer to many questions in the methylammonium lead halide solar cell absorbers. *Adv. Energy Mater.* **7**, 1700600 (2017).
36. Leguy, A. M. et al. The dynamics of methylammonium ions in hybrid organic-inorganic perovskite solar cells. *Nat. Commun.* **6**, 1–11 (2015).
37. Dong, Q. F. et al. Lateral-structure single-crystal hybrid perovskite solar cells via piezoelectric poling. *Adv. Mater.* **28**, 2816–2821 (2016).
38. Rakita, Y., Bar-Elli, O., Meirzadeh, E. & David, C. Tetragonal $CH_3NH_3PbI_3$ is ferroelectric. *Proc. Natl Acad. Sci. USA* **114**, E5504–E5512 (2017).
39. Röhm, H., Leonhard, T., Hoffmann, M. J. & Colsmann, A. Ferroelectric domains in methylammonium lead iodide perovskite thin-films. *Energy Environ. Sci.* **10**, 950–955 (2017).
40. Kutes, Y. et al. Direct observation of ferroelectric domains in solution-processed $CH_3NH_3PbI_3$ perovskite thin films. *J. Phys. Chem. Lett.* **5**, 3335–3339 (2014).
41. Liu, Y. et al. Chemical nature of ferroelastic twin domains in $CH_3NH_3PbI_3$ perovskite. *Nat. Mater.* **17**, 1013–1019 (2018).

42. Zhang, Y., Jie, W., Chen, P., Liu, W. & Hao, J. Ferroelectric and piezoelectric effects on the optical process in advanced materials and devices. *Adv. Mater.* **30**, 1707007 (2018).

43. Weller, M. T., Weber, O. J., Henry, P. F., Di Pumpo, A. M. & Hansen, T. C. Complete structure and cation orientation in the perovskite photovoltaic methylammonium lead iodide between 100 and 352 K. *Chem. Commun.* **51**, 4180–4183 (2015).

44. Kawamura, Y., Mashiyama, H. & Hasebe, K. Structural study on cubic-tetragonal transition of $CH_3NH_3PbI_3$. *J. Phys. Soc. Jpn.* **71**, 1694–1697 (2002).

45. Gómez, A., Wang, Q., Goñi, A. R., Campoy-Quiles, M. & Abate, A. Ferroelectricity free lead halide perovskites. *Energy Environ. Sci.* **12**, 2537–2547 (2019).

46. Frohna, K. et al. Inversion symmetry and bulk rashba effect in methylammonium lead iodide perovskite single crystals. *Nat. Commun.* **9**, 1–9 (2018).

47. Shahrokhi, S. et al. Emergence of ferroelectricity in halide perovskites. *Small Methods* **4**, 2000149 (2020).

48. Huang, B. Y. et al. Polar or nonpolar? That is not the question for perovskite solar cells. *Natl. Sci. Rev.* **8**, nwab094 (2021).

49. Lovinger, A. J. Ferroelectric polymers. *Science* **220**, 1115–1121 (1983).

50. Motta, C. et al. Revealing the role of organic cations in hybrid halide perovskite $CH_3NH_3PbI_3$. *Nat. Commun.* **6**, 7026 (2015).

51. Lee, J. H. et al. Resolving the physical origin of octahedral tilting in halide perovskites. *Chem. Mat.* **28**, 4259–4266 (2016).

52. Lee, J.-H., Bristowe, N. C., Bristowe, P. D. & Cheetham, A. K. Role of hydrogen-bonding and its interplay with octahedral tilting in $CH_3NH_3PbI_3$. *Chem. Commun.* **51**, 6434–6437 (2015).

53. Breternitz, J., Lehmann, F., Barnett, S. A., Nowell, H. & Schorr, S. Role of the iodide-methylammonium interaction in the ferroelectricity of $CH_3NH_3PbI_3$. *Angew. Chem. Int. Ed.* **59**, 424–428 (2020).

54. Lee, J. H., Lee, J. H., Kong, E. H. & Jang, H. M. The nature of hydrogen-bonding interaction in the prototypic hybrid halide perovskite, tetragonal $CH_3NH_3PbI_3$. *Sci. Rep.* **6**, 1–12 (2016).

55. Fan, N., Ma, X. & Xu, B. Effect of iodine octahedral rotation on dipole ordering in organic-inorganic hybird perovskite $CH_3NH_3PbI_3$. *J. Phys. Chem. C* **126**, 779–785 (2022).

56. Boström, H. L. B., Senn, M. S. & Goodwin, A. L. Recipes for improper ferroelectricity in molecular perovskites. *Nat. Commun.* **9**, 2380 (2018).

57. Gómez-Aguirre, L. C. et al. Room-temperature polar order in $[NH_4][Cd(HCOO)_3]$—a hybrid inorganic-organic compound with a unique perovskite architecture. *Inorg. Chem.* **54**, 2109–2116 (2015).

58. Hu, K. L., Kurmoo, M., Wang, Z. & Gao, S. Metal-organic perovskites: synthesis, structures, and magnetic properties of $[C(NH_2)_3][MII(HCOO)_3](M=$ Mn, Fe, Co, Ni, Cu, and Zn; $C(NH_2)_3=$ guanidinium). *Chem. Eur. J.* **15**, 12050–12064 (2009).

59. Stroppa, A. et al. Electric control of magnetization and interplay between orbital ordering and ferroelectricity in a multiferroic metal-organic framework. *Angew. Chem. Int. Ed.* **50**, 5847–5850 (2011).

60. Collings, I. E. et al. Compositional dependence of anomalous thermal expansion in perovskite-like ABX_3 formates. *Dalton Trans.* **45**, 4169–4178 (2016).

61. Wu, Y. et al. $[Am]Mn(H_2POO)_3$: a new family of hybrid perovskites based on the hypophosphite ligand. *J. Am. Chem. Soc.* **139**, 16999–17002 (2017).

62. Wei, H., Yang, Y. L., Chen, S. Y. & Xiang, H. J. Lead-free hybrid perovskite $N(CH_3)_4SnI_3$ with robust ferroelectricity induced by large and non-polar $N(CH_3)_4^+$ molecular cation. *Nat. Commun.* **12**, 1–8 (2021).

63. Goldschmidt, V. M. Die gesetze der krystallochemie. *Sci. Nat.* **14**, 477–485 (1926).

64. Randall, C. A., Bhalla, A. S., Shrout, T. R. & Cross, L. E. Classification and consequences of complex lead perovskite ferroelectrics with regard to B-site cation order. *J. Mater. Res.* **5**, 829–834 (1990).

65. Dimesso, L., Wussler, M., Mayer, T., Mankel, E. & Jaegermann, W. Inorganic alkali lead iodide semiconducting $APbI_3$ (A= Li, Na, K, Cs) and NH_4PbI_3 films prepared from solution: structure, morphology, and electronic structure. *AIMS Mater. Sci.* **3**, 737–755 (2016).

66. Xi, R., Skelton, J. M., da Silva, E. L., Frost, J. M. & Walsh, A. Spontaneous octahedral tilting in the cubic inorganic caesium halide perovskites $CsSnX_3$ and $CsPbX_3$ (X = F, Cl, Br, I). *J. Phys. Chem. Lett.* **8**, 4720–4726 (2017).

67. Kieslich, G., Sun, S. & Cheetham, A. K. Solid-state principles applied to organic-inorganic perovskites: new tricks for an old dog. *Chem. Sci.* **5**, 4712–4715 (2014).

68. Glazer, A. M. The classification of tilted octahedra in perovskites. *Acta Crystallogr. B* **B28**, 3384–3392 (1972).

69. Hohenberg, P. & Kohn, W. Inhomogeneous electron gas. *Phys. Rev.* **136**, B864 (1964).

70. Kohn, W. & Sham, L. J. Self-consistent equations including exchange and correlation effects. *Phys. Rev.* **140**, A1133 (1965).

71. Kresse, G. & Furthmüller, J. Efficiency of ab-initio total energy calculations for metals and semiconductors using a plane-wave basis set. *Comput. Mater. Sci.* **6**, 15–50 (1996).

72. Kresse, G. & Furthmüller, J. Efficient iterative schemes for ab initio total-energy calculations using a plane-wave basis set. *Phys. Rev. B* **54**, 11169 (1996).

73. Blöchl, P. E. Projector augmented-wave method. *Phys. Rev. B* **50**, 17953 (1994).

74. Kresse, G. & Joubert, D. From ultrasoft pseudopotentials to the projector augmented-wave method. *Phys. Rev. B* **59**, 1758 (1999).

75. Perdew, J. P., Burke, K. & Ernzerhof, M. Generalized gradient approximation made simple. *Phys. Rev. Lett.* **77**, 3865–3868 (1996).

76. Perdew, J. P., Burke, K. & Ernzerhof, M. Generalized gradient approximation made simple. *Phys. Rev. Lett.* **78**, 1396 (1997).

77. Perdew, J. P. et al. Restoring the density-gradient expansion for exchange in solids and surfaces. *Phys. Rev. Lett.* **100**, 136406 (2008).

78. Togo, A., Oba, F. & Tanaka, I. First-principles calculations of the ferroelastic transition between rutile-type and $CaCl_2$-type SiO_2 at high pressures. *Phys. Rev. B* **78**, 134106 (2008).

79. Parlinski, K., Li, Z. Q. & Kawazoe, Y. First-principles determination of the soft mode in cubic ZrO_2. *Phys. Rev. Lett.* **78**, 4063–4066 (1997).

80. Resta, R. Macroscopic polarization in crystalline dielectrics: the geometric phase approach. *Rev. Mod. Phys.* **66**, 899 (1994).

81. King-Smith, R. D. & Vanderbilt, D. Theory of polarization of crystalline solids. *Phys. Rev. B* **47**, 1651 (1993).

82. Henkelman, G., Uberuaga, B. P. & Jonsson, H. A climbing image nudged elastic band method for finding saddle points and minimum energy paths. *J. Chem. Phys.* **113**, 9901–9904 (2000).

83. Grimme, S., Antony, J., Ehrlich, S. & Krieg, H. A consistent and accurate ab initio parametrization of density functional dispersion correction (DFT-D) for the 94 elements H-Pu. *J. Chem. Phys.* **132**, 154104 (2010).

ACKNOWLEDGEMENTS

AUTHOR CONTRIBUTIONS

J.-Z.Z. conceived the original ideas and supervised the project. J.-B.L. and Z.-K.J. performed the calculations. J.-B.L., Z.-K.J. and J.-Z.Z. prepared the manuscript. R.W. joined the discussions of the whole project.

COMPETING INTERESTS

The authors declare no competing interests.

ADDITIONAL INFORMATION

Supplementary information The online version contains supplementary material available at https://doi.org/10.1038/s41524-023-01019-2.

Correspondence and requests for materials should be addressed to Jin-Zhu Zhao or Ruiqiang Wang.

Reprints and permission information is available at http://www.nature.com/reprints

Publisher's note Springer Nature remains neutral with regard to jurisdictional claims in published maps and institutional affiliations.